POLISH POLAR RESEARCH
vol. 47 no. 1–2, pp. 1–12
DOI: 10.24425/ppr.2026.158405

Magnetic image of the Ezcurra Inlet and its geological interpretation (King George Island, Western Antarctica)

Jerzy NAWROCKI[1,2]*, Marcin OLKOWICZ[3], Zdzisław PETECKI[1], Jakub BAZARNIK[4], Weronika CZARNECKA[1] and Tomasz KURCZABA[5]

[1]*Polish Geological Institute – National Research Institute, Rakowiecka 4, 00-975 Warszawa, Poland*

[2]*Institute of Earth and Environmental Sciences, Maria Curie-Skłodowska University in Lublin, Kraśnicka 2d, 20-718 Lublin, Poland*

[3]*Polish Geological Institute – National Research Institute, Lower Silesian Branch, Jaworowa 19, 53-122 Wrocław, Poland*

[4]*Polish Geological Institute - National Research Institute, Carpathian Branch, Skrzatów 1, 31-560 Kraków, Poland*

[5]*Department of Antarctic Biology, Institute of Biochemistry and Biophysics, Polish Academy of Sciences, Pawińskiego 5a, 02-106 Warszawa, Poland*

***corresponding author:** *jnaw@pgi.gov.pl*

Received 28 April 2026 **Accepted** 23 June 2026

Abstract: A magnetic map of the Ezcurra Inlet area on King George Island and magnetic parameters from some adjacent rocks are presented and interpreted herein. A set of local distinct magnetic anomalies stretching in the SE coast of Ezcurra Inlet and located on faults transverse to the Ezcurra Fault was defined. At least part of them define location of volcanic activity centers. A linear arrangement of anomalies indicates that the fault or fracture parallel to the Ezcurra Fault in sites crossed by transverse faults opened up magma migration paths. The map of regional magnetic anomalies, similarly to the previous seismic data, indicate that the deeply rooted Ezcurra Fault turns in western Ezcurra Inlet to the NW. This non-straight course does not support its simple strike-slip nature at least in this part of the island.

Keywords: Antarctic, South Shetlands, magnetic survey, faulting, geology.

Introduction

King George Island (KGI), the biggest island of the South Shetland Islands (SSI) archipelago (Fig. 1A), is dominated by volcanic and plutonic rocks, with subsidiary areas of fore-arc and intra-arc sedimentary rocks (Smellie *et al.* 1984; Smellie 2021; Bastias *et al.* 2023). It is located at the southern margin of the South Scotia Ridge. The geological structures of SSI were formed during the subduction of the Phoenix Plate under the Antarctic Plate from the Triassic to the middle Miocene (Pankhurst and Smellie 1983; Willan and Kelley 1999; Bastias *et al.* 2020; Smellie 2021; Bastias-Silva *et al.* 2024). They were detached from the Antarctic Peninsula in the Pliocene (Barker 1982; Barker and Dalziel 1983; Pańczyk and Nawrocki 2011) due to tectonic extensional processes leading to the opening of the Bransfield Strait. Birkenmajer (1983) distinguished four major tectonic blocks of KGI separated by longitudinal strike-slip faults: the axial Barton Horst, the northern Fildes Block, the southern Warszawa Block, and the southernmost Kraków Block (Fig. 1B). One of these strike-slip faults, the Ezcurra Fault (EF), is interpreted by Birkenmajer (2002, 2003) as right-lateral strike-slip with the motion that began at *ca.* 54 Ma and continued for a period of at least 21 Ma up to the cessation of subduction (Burton-Johnson *et al.* 2023).

Studies of the anisotropy of magnetic susceptibility of the rocks located in the vicinity of the EF do not support the thesis about large scale dextral tectonic transport along this fault and the terrane model of this part of KGI. Most probably this fault has not acted as the large strike-slip at least since the late Eocene (Nawrocki and Werner 2025). The deep nature of the EF was documented by the seismic experiment (Majdański *et al.* 2008). However, good quality data allowing to trace its course covered only a small

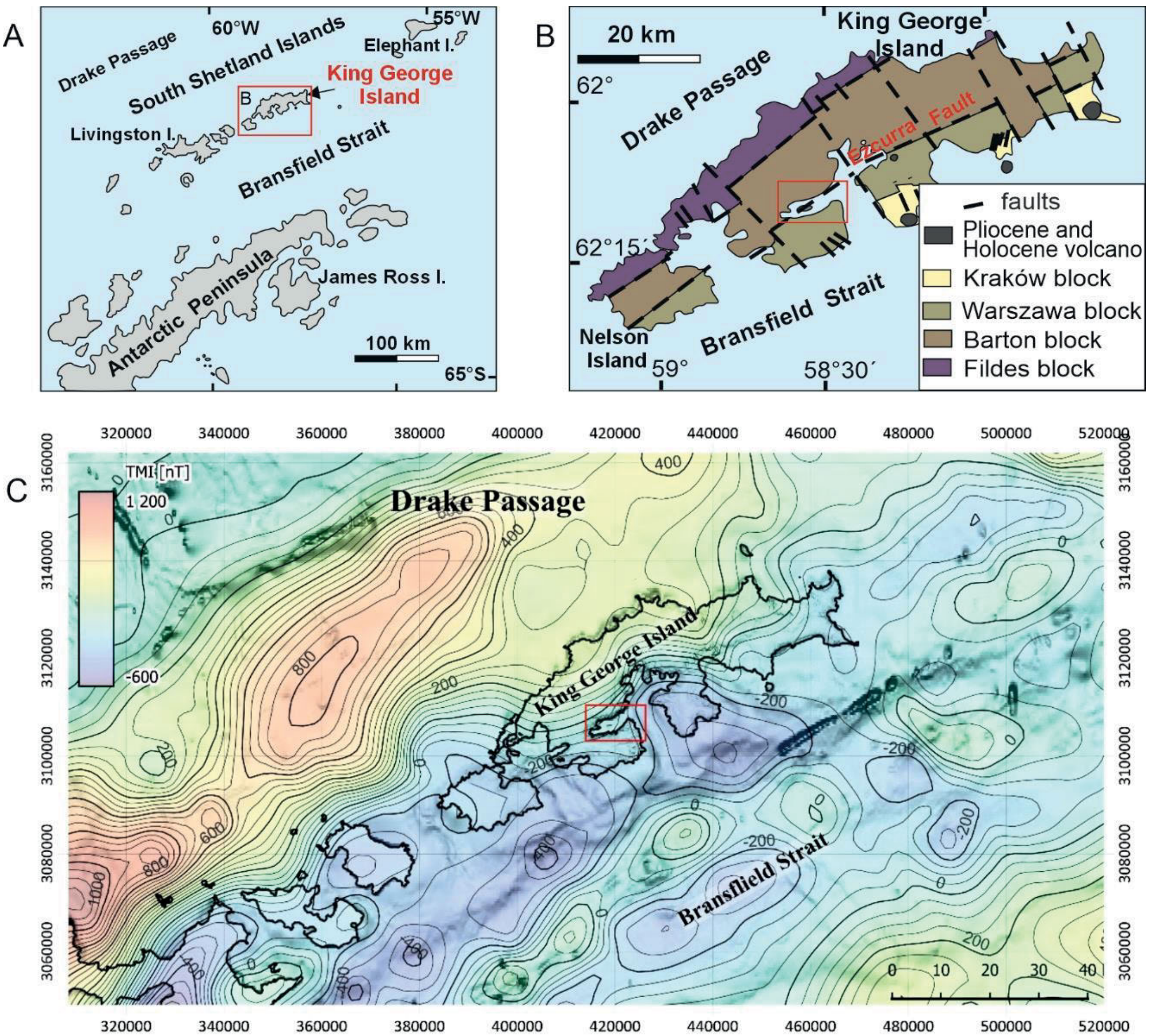

Fig. 1. Location of study area; **A** – general location of King George Island; **B** – major tectonic division of King George Island according to Birkenmajer (1983); **C** – regional magnetic anomaly map based on ADMAP2 (Golynsky *et al.* 2018).

part of it. A system of numerous strike-slip faults, transverse to the longitudinal main faults and somewhere penetrated by Late Oligocene to Miocene dyke intrusions of the Admiralty Bay Group (Birkenmajer 1983; Pańczyk *et al.* 2009) was developed in the Ezcurra Inlet (EI) and the adjacent areas. Angular unconformities are observed between particular volcanogenic formations and even inside them. For example, an unconformity of *ca.* 25º was observed in the EI at Dufayel Island (Birkenmajer 2002). It should be stressed, however, that these angular unconformities may not be exclusively of tectonic origin but they can result from a change in the location of magma source.

The tectonic evolution of KGI has been studied by Tokarski (1987). He stated that brittle deformations prevail in the late Mesozoic through the recent volcanic sequence of KGI, and shear deformations predominate over extensional ones. Kraus *et al.* (2010) and Burton–Johnson *et al.* (2023) noted that the peak of intrusive activity at KGI 47–45 Ma ago coincided with a dramatic change in subduction zone parameters that caused a change from a compressional to an extensional tectonic regime.

The geomagnetic measurements and their analysis in the SSI and adjacent areas were performed mostly on a large scale with a focus on regional crustal structures mostly related to Phoenix plate subduction or back-arc basin evolution and recent volcanic activity at Bransfield Strait (Yegorova *et al.* 2011; Catalán *et al.* 2013; Almendros *et al.* 2020; Espinoza Celi *et al.* 2023). Espinoza Celi *et al.* (2023) used ADMAP2 (Golynsky *et al.* 2018) 1.5 km gridded magnetic anomaly map (Fig. 1C) covering the entire area to describe major tectonic features of SSI and Bransfield Strait. The ADMAP2 grid and its raw data are free access bases produced from near surface measurements (airborne and shipborne), yet none of the raw profile lines go through Admiralty Bay or KGI. High resolution magnetic shipborne data of Almendros *et al.* (2020) covered the areas of Orca Volcano, Humpback Volcano, and Three Sisters Edifice of the Bransfield Strait Rift system, not reaching Admiralty Bay.

The age of most of the rock formations adjacent to the EI (Fig. 2) has been precisely defined thanks to extensive isotope $^{238}U/^{206}Pb$ and $^{40}Ar/^{39}Ar$ studies. The Znosko Gla-

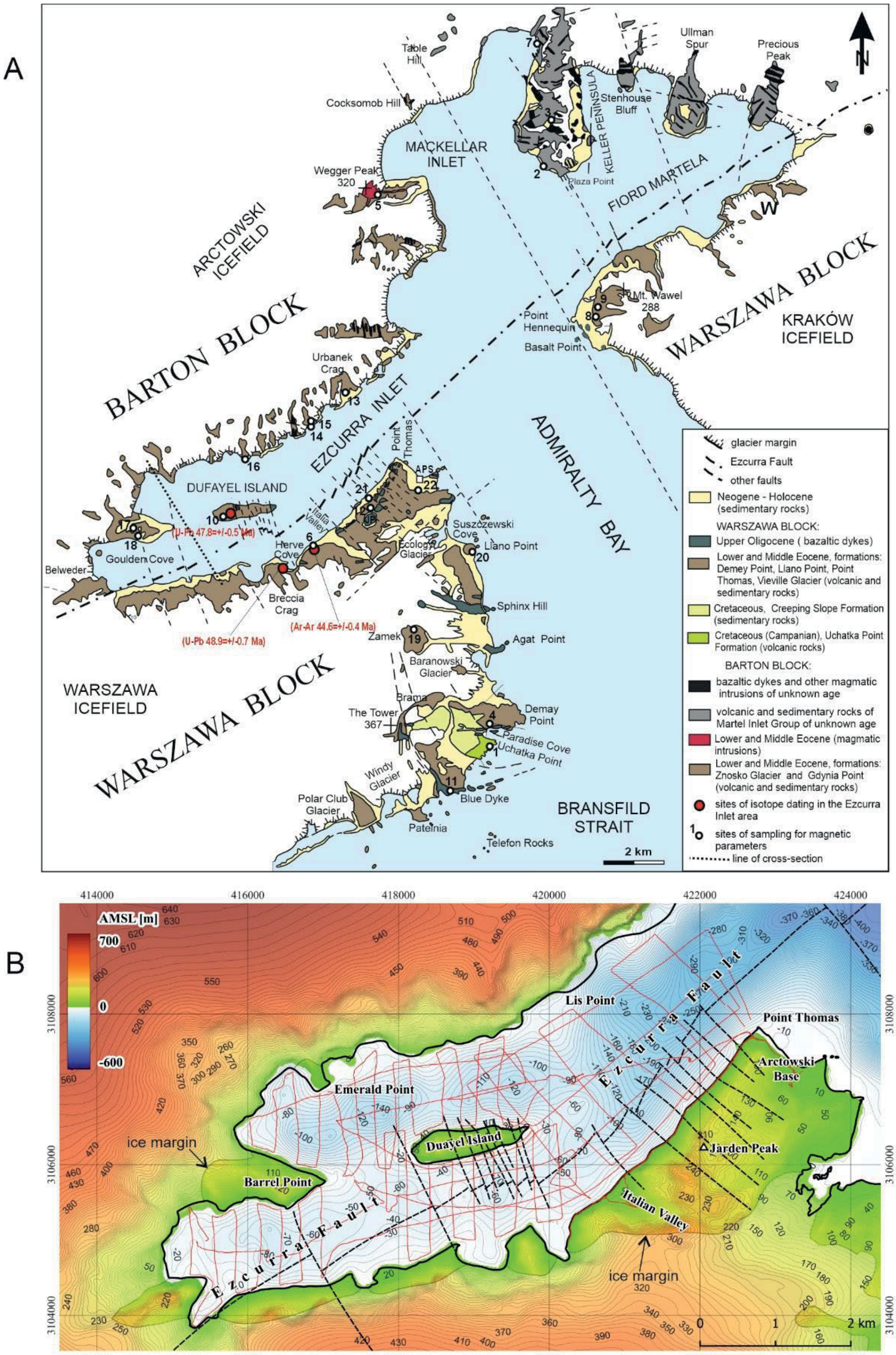

Fig. 2. Geology and topography of study area; **A** – sites of sampling for magnetic parameters on the background of geological map of central part of King George Island, after Birkenmajer 2002, simplified and with ages of particular lithostratigraphic units corrected by Nawrocki *et al.* (2010, 2021), magnetic parameters measured for particular sites are listed in Table 1; **B** – magnetic measurement (red lines) on hypso- and bathymetry of Ezcurra Inlet (Tozer *et al.* 2019).

cier Formation cropping out at Dufayel Island was dated at 47.8 ± 0.5 (Nawrocki *et al.* 2010). The section extending from the Italian Valley along the Dutkiewicz Cliff provided $^{40}Ar/^{39}Ar$ isotope ages of 44.9 ± 0.7 Ma and 44.6 ± 0.4 Ma, based on 16 drill samples (Nawrocki *et al.* 2010). On the other hand, the basaltic trachyandesites from the Herve Cove were dated at 48.9 ± 0.5 Ma with the $^{238}U/^{206}Pb$ method (Nawrocki *et al.* 2011). Two geological units, the Vieville Glacier and Mount Wawel formations (Birkenmajer 2003), redefined and incorporated into the Hennequin Formation by Smellie *et al.* (2021) were dated at 48.7 ± 0.6 Ma and 45.3 ± 0.3 Ma, respectively (Nawrocki *et al.* 2011). The Jardine Peak large vertical intrusion took place 25.4 ± 0.4 Ma ago, *i.e.*, during the Late Oligocene (Chattian) (Pańczyk *et al.* 2009).

In this paper, we present a new magnetic map of the EI and magnetic parameters from adjacent rock formations. Taking into consideration these data, previously published result of seismic studies (Majdański *et al.* 2008) and existing tectonic/stratigraphic interpretations, we aimed to verify some basic geological features of the EI area, among them the course of the EF and the location of volcanic centers. This research is a part of a broader research program aiming for geophysical mapping of subglacial and submarine geological structures of KGI.

Methods

Acquisition and preparation of magnetic data

Field measurements were acquired by boat and land surveys during the 49th Polish Antarctic Expedition in early 2025. Measurements were carried out with Geometrics MagArrow, a high-precision laser-pumped cesium total magnetic field magnetometer designed for drone-based work. As the MagArrow is a drone agnostic device, it can operate independently, allowing different usage. For the boat borne measurements, the MagArrow magnetometer was placed in a plastic pipe of *ca.* 50 cm diameter closed at both ends to protect it from the potential saltwater splashes. Then the entire assembly was secured on the aluminum bottom pontoon towed 20 m behind the Zodiac motorboat. In this setup, electromagnetic noise produced by the motor engine and electronics on the motorboat was minimized, while still allowing to safe maneuvering between ice patches (Fig. 3).

To remove diurnal variation, all measurements were corrected using data from the proton precision magnetometer base station. The base station was always placed at the same point a few hundred meters from the Arctowski Station. High frequency noise was removed using lowpass filtering with a cutoff frequency of 5 seconds performed on raw data. To reduce remaining heading error of up to 15 nT on lines crossing points, boat-borne surveys were leveled by minimizing misfit between "lines" and "tie lines". The same operation was performed to fit data from adjacent surveys using overlapping areas.

As the land survey has no crossing points, the heading error was removed by performing calibration measurements at the same point with different magnetometer orientations. Assuming constant magnetic field at point over the time of calibration, that depends only on magnetometer orientation, the correction data were created. They were subtracted from the measured field based on local magnetometer orientation. Combined data from boat and land

Fig. 3. Magnetometer setup for boat borne magnetic measurements in the Ezcurra Inlet.

measurements were interpolated onto a 10 m spacing regular grid. The International Geomagnetic Reference Field Generation 14 (IGRF-14) was used to calculate geomagnetic anomalies.

Data processing

Processing magnetic field data involves applying various filters to highlight certain features of the data. The reduction to the pole method (RTP), and the regional-residual separation of the RTP were applied to the magnetic TMI data. The RTP transformation was used to recalculate the magnetic anomaly into the anomaly that would be observed at the north magnetic pole, where the geomagnetic field and the respective induced magnetization vector is vertical (Baranov 1957; Baranov and Naudy 1964). This procedure facilitates the interpretation of the data because the RTP transformation shifts the anomaly laterally to be centered over the source of the anomaly. The magnetic data were transformed by the RTP transformation, assuming the average direction of total magnetization of most rocks to be parallel or anti-parallel to the Earth's main field (inclination = −55.7, declination = 10.1 for the study area). However, the strong remanent magnetization of rocks may cause errors in the interpretation of magnetic data due to deviation from the induced magnetization.

The magnetic field represents the sum of a series of anomalies caused by deep and shallow sources referred to as regional and residual or local anomalies. Regional residual separation was used to reveal the major structures of the basement and enhance the expression of local anomalies originating from hidden basement structures (Blakely 1996). Various techniques for regional residual separation are described (Nabighian *et al.* 2005). The magnetic anomaly separation methodology used in this work applies spectral analysis and wavelength filtering. In this case, deeper sources would be associated with long wavelength (regional) anomalies, while the shallower sources would be associated with short wavelength (residual or local) anomalies. The regional and residual RTP anomalies are calculated using a low-pass and high-pass Butterworth filter with a cut-off wavelength of 2000 m, based on the slope of the radially averaged power spectrum (Spector and Grant 1970). As there is no universal rule to separate local and regional anomalies, the cut-off wavelength chosen for this particular case also was based on geology, topography and size of the study area.

Assuming that the study area of roughly 4 x 10 km consists of two major magnetic domains separated by EF, and that the EI maximum depth reaches 400 m, a lowpass filter with a cut-off wavelength of 2000 m should, first reduce the effect of variable source-to-sensor distance caused by water depth changes, and second produce regional maps with only a few major anomalies related to the deepest, largest bodies related to the scope of this investigation. This cut-off wavelength also ensures that the observed regional anomalies were measured on at least several adjacent survey lines. Analogously, residual maps should cover most of the local anomalies and artifacts filtered from the regional anomaly maps. Regional and residual RTP anomalies allow the creation of magnetic maps that highlight regional structures in the basement of the EI or depict local structures in the uppermost part of the basement.

Rock magnetic and palaeomagnetic parameters

A total of 22 geographically oriented hand samples and drill samples were taken in central-southern KGI (Fig. 2). They were cut into specimens one inch in diameter and 22 mm long. The intensity and the direction of natural remanent magnetization were measured using a JR-6A spinner magnetometer (AGICO Brno). For the calculations of these parameters, the REMASOFT software from AGICO Brno has been used. The magnetic susceptibility and its anisotropy (not presented here) were measured by means of an MKF1-FB bridge (AGICO Brno). Data obtained from at least three specimens for each locality are listed in Table 1.

Results

Magnetic survey

TMI anomalies in the survey area range from −1800 to 4100 nT (Fig. 4A). From the outlook of the TMI map and the RTP magnetic map (Fig. 4B), the RTP transformation resulted in a SW displacement of the anomaly peaks, compensating for the northward shift induced by the negative inclination and the eastward skewness resulting from the positive declination at the study area. The RTP magnetic anomalies are characterized by diverse amplitudes, shapes, polarizations, and relief that reflect sources at different crustal levels. Their majority is characterized by moderate amplitude and gradient, especially in the western part of the study area. A series of short wavelength, high amplitude anomalies is concentrated over the SE coast of EI (Fig. 4B). In the NE part of the study area, there is a widespread, moderate minimum, bounded to the south by a broad gradient zone and moderate magnetic highs. This magnetic pattern may be partly related to the deepening of the seabed to −400 m and the relatively sparse offshore survey lines, which cause a decrease in the resolution of its magnetic imaging.

The high-pass filter applied to the RTP magnetic map data indicates a number of regular to elongate and curvilinear short wavelength magnetic anomalies (Fig. 5A). Anomalies with very high amplitudes (−1700–3300 nT) and steep magnetic gradients are located along the SE coast of EI. Also, the map contains lower amplitude anomalies bounded by more gradational magnetic gradient zones. An interesting feature is the elongate anomaly located in the eastern part of the studied area.

The RTP magnetic map with a low-pass filter shows regional large-amplitude positive anomalies (*ca.* 300–400 nT) occurring along the southern coast of EI and in the NW part of the study area (Fig. 5B). In the

Table 1. Volume magnetic susceptibility and natural remanent magnetization (NRM) parameters of selected rocks from the Admiralty Bay area of King George Island

No	Unit	Type of rock, age	Area of study, sample coordinates	Volume magnetic susceptibility (x 10^{-3} SI u.)	Intensity of NRM (x 10^{-2} A/m)	Declination/ inclination of NRM
1.	Uchatka Point Formation	basalt, 75.4 Ma	Uchatka Point – Paradise Cove: 62° 13′ 30″ S 58° 26′ 27″ W	54.8	90.3	340/−80
2.	Keller Peninsula Formation	basaltic andesite, 60.6 Ma	Keller Peninsula: 62° 5′ 24.06″ S 58° 24′ 29.76″ W	38.1	22.5	151/35
3.	Visca Anchorage Formation	basaltic andesite, 54–50 Ma	Keller Peninsula: 62° 4′ 26.1″ S 58° 24′ 51.12″ W	36.1	14.2	130/50
4.	Demay Point Formation	trachyte, 51.6–53 Ma	Demay Point –Paradise Cove: 62° 13′ 12″ S 58° 25′ 55″ W	33.6	12.3	315/−67
5.	Weger Peak Group	diorite, 49.1 Ma quartz diorite	Weger Peak: 62° 05′ 21″ S 58° 29′ 42″ W	78.8 34.3	430 120	200/61 190/64
6.	Point Thomas Formation	basaltic andesite, trachybasalt, 47.8–48.9 Ma	Italian Valley – Herve Cove 62° 10′ 25″ S 58° 31′ 15″ W	58.1	43.6	345/−62
7.	Domeyko Glacier Formation	andesite, 45.8–48.7 Ma	Keller Peninsula: 62° 03′ 47.1″ S 58° 24′ 53.34″ W	15.5	6.7	135/−65
8.	Vieville Glacier Formation	basaltic andesite, 46.7 Ma	Mount Wawel: 62° 07′ S5″ S 58 23′12″ W	67.2	81.2	80/75
9.	Mount Wawel Formation	basaltic andesite, 45 Ma	Mount Wawel: 62° 07′ 46″ S 58° 23′ 10″ W	48.8	48.3	105/85
10.	Znosko Glacier Formation	andesite, 45.1 Ma	Dufayel Island: 62° 09′ 55″ S 58° 34′ 25″ W	10.6	8.1	340/−68
11.	Admiralty Bay Group, Spinx Hill Dykes	basaltic andesite, 27.9 Ma	Blue Dyke: 62° 13′ 47″ S 58° 27′ 30″ W	50.4	23.8	358/−71
12.	Arctowski Cove Formation	basaltic andesite, *ca.* 49 Ma	SE Ezcurra Inlet: 62° 10′ 18.67″ S 58° 29′ 24.71″ W	39.9	226	347/−58
13.	Znosko Glacier Formation	andesite, *ca.* 48 Ma	Urbanek Crag, NE Ezcurra Inlet: 62° 08′ 19.46″ S 58° 30′ 24.07″ W	24.2	27.3	12/−9
14.	Znosko Glacier Formation	basaltic andesite, *ca.* 48 Ma	Lis Point, N Ezcurra Inlet: 62° 08′ 27.14″ S 58° 31′ 13.41″ W	45.9	42.1	287/−29
15.	Znosko Glacier Formation	basalt, *ca.* 48 Ma	Lis Point, N Ezcurra Inlet: 62° 08′ 27.07″ S 58° 31′ 13.39″ W	66.8	60.6	228/−7
16.	Znosko Glacier Formation	basaltic andesite, *ca.* 48 Ma	Ladies Buttresses, N Ezcurra Inlet 62° 06′ 36.03″ S 58° 25′ 31.93″ W	51.8	21.9	286/−3

Table 1 continued

No	Unit	Type of rock, age	Area of study, sample coordinates	Volume magnetic susceptibility (x 10^{-3} SI u.)	Intensity of NRM (x 10^{-2} A/m)	Declination/ inclination of NRM
17.	Dalmor Bank Formation	tuffaceous rocks, *ca.* 45 Ma?	Goulden Cove, W Ezcurra Inlet: 62° 10′ 10.39″ S 58° 36′ 0.79″ W	7.2	6.2	323/−12
18.	Gdynia Point Formation	basaltic andesite agglomerate, *ca.* 48 Ma?	Barrel Point, W Ezcurra Inlet: 62° 10′ 12.86″ S 58° 35′ 33.67″ W	21.1	19.9	357/−13
20.	Llano Point Formation	basaltic andesite, *ca.* 50 Ma	Llano Point, W Admiralty Bay: 62° 11′ 45.71″ S 58° 28′ 7.52″ W	15.9	291	300/39
21.	Point Thomas Formation	basalt, *ca.* 49 Ma	S Ezcurra Inlet: 62° 10′ 13.61″ S 58° 30′ 55.3″ W	41.7	84.7	344/−63
22.	Petrified Forest Member, Arctowski Cove Formation	tuffaceous sandstone	Arctowski Polish Antarctic Station: 62° 9′ 43.57″ S 58° 28′ 13.84″ W	10.1	17.9	125/−77

NE part of the area, a regional anomaly of negative intensity occurs. All these anomalies are clearly separated by gradient zones, which probably represent deep fault zones.

Rock magnetic and palaeomagnetic parameters

The lowest mean volume magnetic susceptibility (7.2–24.2 x 10^{-3} SI units) was measured in samples of andesite from the Dufayel Island (Znosko Glacier Formation), tuffaceous agglomerate from Goulden Cove (Dalmork Bank Formation), tuffaceous sandstone from the vicinity of Arctowski Station (Petrified Forest Member of Arctowski Cove Formation), andesites from Keller Peninsula and Urbanek Crag (Domeyko Glacier and Znosko Glacier formations), and basaltic andesites from Barrel Point and Llano Point (Gdynia Point and Llano Point formations) (Table 1 and Fig. 5A). The highest mean value of this parameter (50.4 −78.8 x 10^{-3} SI) is characteristic for samples of basalts from Lis Point (Znosko Glacier Formation) and Uchatka Point (Uchatka Point Formation), basaltic andesites from the Italian Valley – Herve Cove section (Point Thomas Formation), Mount Wawel (Vieville Glacier Formation), and Blue Dyke (Admiralty Bay Group), and diorite cropping out on Wegger Peak (Wegger Peak Group). Except for the basaltic andesite from Llano Point, the rest of the rocks found a positive, near proportional relationship between their magnetic susceptibility and the intensity of natural remanent magnetization. The values of declination and inclination of natural remanent magnetization, measured for rocks from the southwest coast of EI, correspond to the expected normal polarity field direction and differ substantially from those obtained in samples from the rest of EI, where flat inclination is typical.

Discussion

Magnetic image and magnetic parameters

Most of the local magnetic anomalies of low amplitude from the area northwest of the EF can be linked with the occurrences of andesitic rocks and tufaceous agglomerates. The andesites are characterized by relatively low values of magnetic susceptibility and intensity of natural remanent magnetization (Table 1 and Fig. 4). Their natural remanent magnetization displayed a shallow inclination, most probably resulting from the coexistence of two different polarity magnetization components. Other types of rocks occur on the opposite side of the EF, where a set of distinct negative and positive local anomalies of total magnetic intensity was recognized (Fig. 5A). This area is a place where the sequence of basalts and basaltic andesites with moderate to high values of magnetic susceptibility and intensity of remanent magnetization occur. All examined samples of these rocks show a steep negative inclination, *i. e.*, normal polarity of natural remanent magnetization. It should be stressed, however, that areas with centres of distinct positive magnetic anomalies were not sampled. The two most intense anomalies have been detected in places covered by the sea.

Centres of magma emplacement

None of the local magnetic anomalies are associated with the EF line. A set of several distinct positive and negative local magnetic anomalies stretches along the SE coast of the EI approximately parallel to the EF (Fig. 5A). Two of them, with the highest amplitude, occur in a water-covered area near the Italian Valley and in the entrance of Herve Cove. The lava flows in the coastal zone of western Herve Cove and those SW of the mouth of the Italian Valley dip

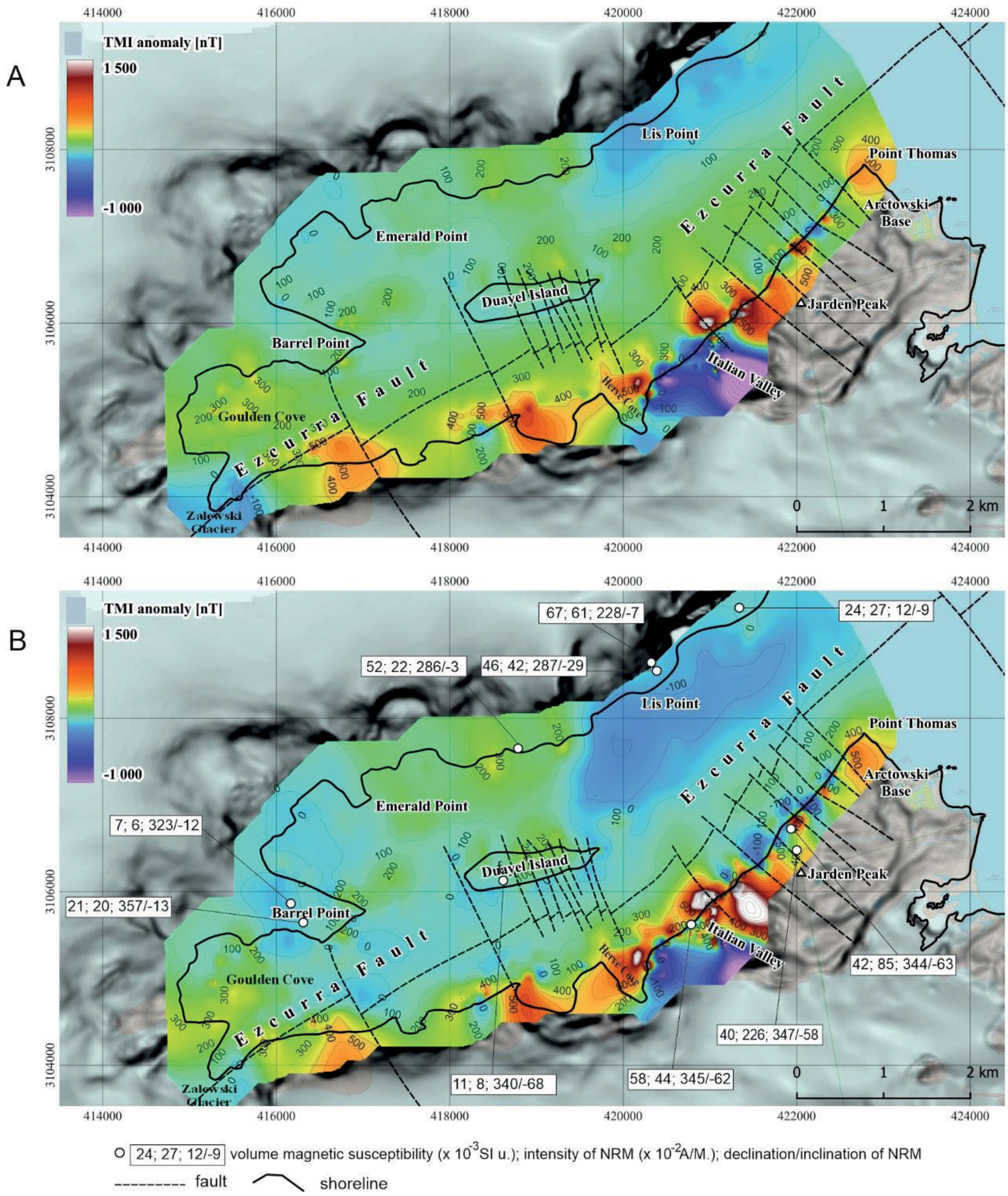

Fig. 4. Magnetic anomalies in the Ezcurra Inlet area. TMI grid (**A**) and TMI grid after RTP correction (**B**). Bold black line indicates shoreline; dashed lines – Ezcurra Fault according to Birkenmajer (2003). The values of magnetic parameters measured for selected sites are also presented.

to the SW (Birkenmajer 2002). Such dip directions mean that these anomalies most probably mark the sites of ancient volcanic eruptions. All distinct local magnetic anomalies on the SE coast of the EI are located on faults transverse to the EF. Their linear arrangement with minor shifts consistent with those marked on the EF by transverse faults (Birkenmajer 2002) can indicate that another fault or fracture, parallel to the EF, here named the Agnes Fracture (Fig. 5A), opened up magma migration paths even before the strike-slip activity of the transverse faults. The Agnes Fracture runs along the SE coast of the EI from Point Thomas to at least Hervé Cove. Currently, it cannot be defined as a fault because there is no evidence of tectonic movements. However, in an alternative solution, it may represent a fault related to the development of the pull-apart basin subsequently infilled by magmatic material.

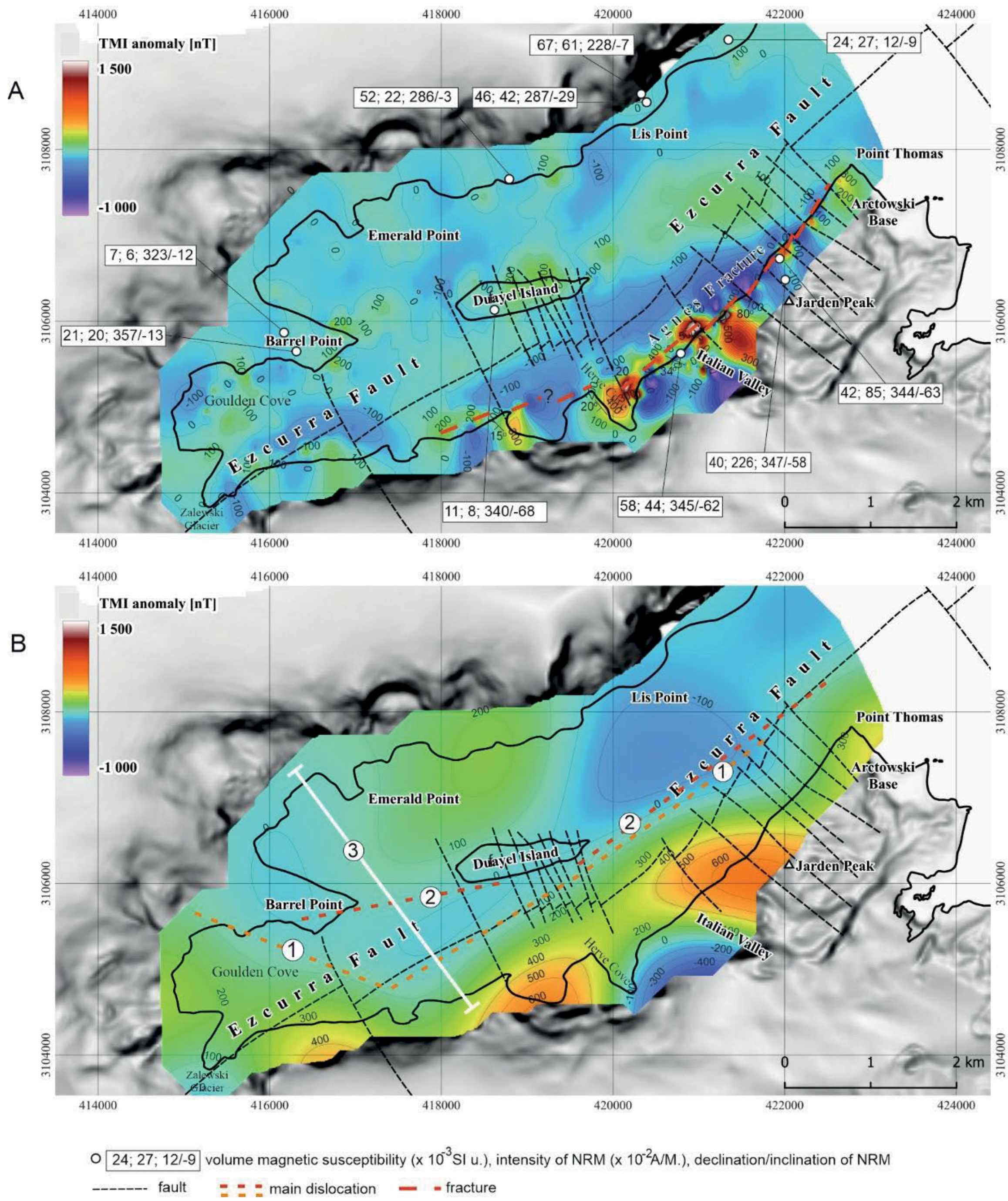

Fig. 5. Magnetic image in the area of Ezcurra Inlet, separated to the local (**A**), and regional (**B**) anomalies, based on RTP corrected data (Fig. 4B). Bold black line shows shoreline; dashed lines – Ezcurra fault according to Birkenmajer (2002); line 1 – approximate course of the deeply rooted regional fault according to magnetic data; line 2 – approximate course of the deeply rooted regional fault according to seismic data (Majdański *et al.* 2008); line 3 – course of cross-section presented in Fig. 6.

According to Birkenmajer (2003), tectonic transport along the EF probably began at *ca.* 54 Ma and continued until *ca.* 21 Ma. In this case, the transverse faults would have to be younger than the volcanogenic sequence from the SE coast of the EI, but this is not the case because its age varying from *ca.* 46 to *ca.* 49 Ma (see Nawrocki *et al.* 2010).

Two belts with low-amplitude positive magnetic anomalies also occur along the EI axis, from the Golden Cove to Dufayel Island and further along its NE coast. However, it is difficult to connect these weak anomalies with any volcanic center. Most probably, it is due to the occurrence of andesites and tuffaceous agglomerates with moderate magnetic susceptibility and intensity of remanent magnetization. The value of total magnetic induction was additionally lowered by a substantial overlapping of secondary magnetization on the primary one, leading to flat inclination and relatively low intensity of natural remanent magnetization.

Course of Ezcurra Fault – seismic *vs.* magnetic data

The course of EF along the EI suggested by Birkenmajer (1982, 2002, 2003) is consistent with the data from seismic studies by Majdański *et al.* (2008) and magnetic data presented here, however, in its eastern and central segments only. Results of seismic experiment indicate that this fault turns in western EI towards Barrel Point (Fig. 5B). Such a substantial change in the direction of EF is supported by regional magnetic anomalies (Fig. 5B). The magnetic high observed in the southern coast of the EI turns to the NW, and it is truncated by the EF drawn by Birkenmajer (2002). This non-straight, *i.e.*, bent course of EF seems to disagree with its simple strike-slip nature suggested by Birkenmajer (2003). It should be stressed, however, that the geological structures of KGI were formed during the oblique subduction of the Phoenix Plate under the Antarctic Plate (Pankhurst and Smellie 1983; Willan and Kelley 1999), and as a consequence, different tectonic domains in this area most probably underwent also a strike slip deformation that, in the EI region, is comparatively subdued. The boundary of the magnetic anomaly in the SW sector of EI and seismic data from this area could define a tectonic lineament oblique to the EF. However, the existence of deep-rotted EF drawn by Birkenmajer (2002) in this area is not supported by seismic and magnetic data.

Majdański *et al.* (2008) distinguished the Barton Horst, with high velocities of 4.5 km s^{-1} in the shallow structures, from Warszawa and Krakow blocks with velocities of 3.5 km s^{-1}, suggesting uplifting the Barton Horst by *ca.* 1.5 km. It should be stressed, however, that both volcanogenic sequences exposed on Dufayel Island within the Barton Horst and in the Herve Cove, belonging to the Warszawa Block, have provided similar zircon $^{238}U/^{206}Pb$ isotope ages of 47.8 ± 0.5 Ma and 48.9 ± 0.7 Ma, respectively (Nawrocki *et al.* 2010). This means that most of the substantial uplift of Barton Horst took place before the emplacement of these rocks, *i.e.*, it is older than the Lutetian.

Bearing in mind magnetic and seismic data alone, the volcanogenic succession from the westernmost part of EI (Goulden Cove area in Fig. 2), defined by Birkenmajer *et al. (*1985) as the Cardozo Cove Group, would have to belong to the Warszawa Block. This unit consists mainly of basic andesite lavas, whereas the volcanogenic sequence of Point Thomas Formation exposed between Italia Valley and Zalewski Glacier (southern coast of EI in Fig. 2) is composed predominantly of basalts (Birkenmajer 2003). The EF, as defined by Birkenmajer (2002, 2003), had to separate two areas with different sources of magma for Eocene volcanogenic rocks. More andesitic sources were situated NW of it. The possibility of two structural complexes of different ages with different boundaries between them and lying at different depths in the western part of EI is therefore likely. The first of them consists of two blocks of older crust separated by a deeply rooted vertical fault identified by seismic data and magnetic survey. The second and younger structural unit is cut by a dislocation, defined by Birkenmajer (1982, 2002) as the continuation of the EF, not mapped in this part of EI by the seismic experiment of Majdański *et al*. (2008). The volcanogenic sequences and vertical intrusions cropping out in this area, *ca.* 49 Ma old and younger, belong to this unit (Fig. 6). The occurrence of older crust on King George Island deduced

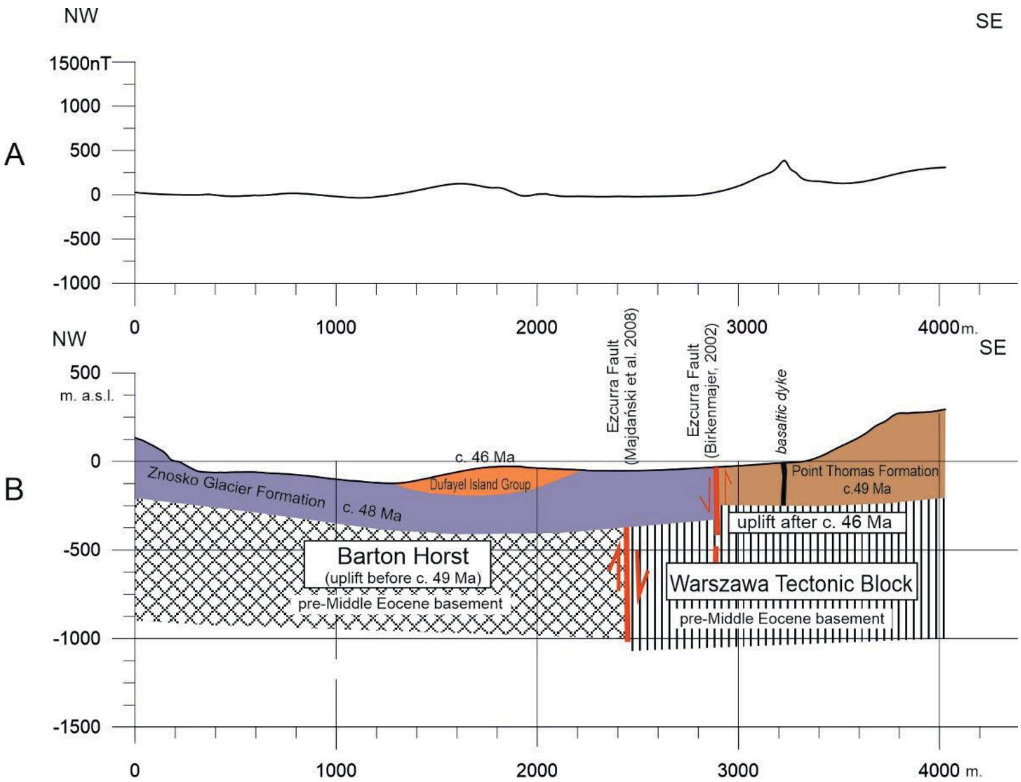

Fig. 6. Magnetic profile (**A**) and simplified conceptual geological cross-section through the Ezcurra Inlet along line 3, as drawn in Fig. 5B (**B**).

from isotope ages of zircon xenocrystals from Eocene to Miocene volcanic rocks has been recently postulated by Xing *et al.* (2025). These authors conclude that the Proterozoic to Cambrian Patagonia crustal fragments may extend into King George Island.

Conclusions

A set of local distinct magnetic anomalies stretching along the SE coast of EI along the line approximately parallel to the EF was disclosed. They are located on faults transverse to the main discontinuity of the EI. A linear arrangement of anomalies indicates that another fault or fracture parallel to this prominent discontinuity opened up magma migration paths in sites crossed by transverse faults. The map of regional magnetic anomalies, similarly to the previous seismic data, may indicate that the EF turns in western EI to the NW. This bent course does not support the strike-slip nature of this deep discontinuity, at least in this part of the island. Geological and geophysical evidence point to the presence of two structural complexes of different ages lying at different depths. The deeper one consists of two blocks of older crust separated by a deeply rooted vertical fault identified by seismic data and magnetic regional anomalies. The younger structural unit, dated at *ca.* 49–46 Ma and younger, cut by another dislocation, consists of volcanogenic sequences and vertical intrusions cropping out in this area.

Acknowledgments

The analytical research and field work was funded by the National Fund for Environmental Protection and Water Management of Poland (project No: 22.9901.2501.00.1). The logistics team of the Arctowski Polish Polar Station (Institute of Biochemistry and Biophysics, Polish Academy of Sciences) are acknowledged for their support during field work. We thank Joaquin Bastias and two anonymous reviewers for their constructive review.

References

Almendros J., Wilcock W., Soule D. *et al.* 2020. BRAVOSEIS: Geophysical investigation of rifting and volcanism in the Bransfield Strait, Antarctica. *Journal of South American Earth Sciences* 104: 102834, doi: 10.1016/j.jsames.2020.102834.

Baranov V. 1957. A new method for interpretation of aeromagnetic maps: Pseudogravity anomalies. *Geophysics* 22: 359–383.

Baranov V. and Naudy H. 1964. Numerical calculation of the formula of reduction to the magnetic pole. *Geophysics* 29: 67–79.

Barker P.F. 1982. The Cenozoic subduction history of the Pacific margin of the Antarctic Peninsula: Ridge crest–trench interactions. *Journal of the Geological Society* 139: 787–801, doi: 10.1144/gsjgs.139.6.0787.

Barker P.F. and Dalziel I.W.D. 1983. Progress in geodynamics in the Scotia Arc region. *In:* Cabre, R. (ed.) *Geodynamics of the Eastern Pacific Region, Caribbean and Scotia Arcs*. *American Geophysical Union, Geodynamics Series* 9: 137–170.

Bastias J., Spikings R., Ulianov A., Burton-Johnson A., Chiaradia M., Baumgartner L., Hervé F., Bouvier A-S. 2020. The Gondwanan margin in west Antarctica: Insights from late Triassic magmatism of the Antarctic Peninsula. *Gondwana Research* 81: 1–20.

Bastias J., Chew D., Villanueva C. *et al.* 2023. The South Shetland Islands, Antarctica: Lithostratigraphy and geological map. *Frontiers in Earth Science* 10: 1002760, doi: 10.3389/feart.2022.1002760.

Bastias-Silva J., Chiaradia M., Burton-Johnson A., Chew D., Riley T. and Jara W. 2024. A temporal control on the isotopic compositions of the Antarctic Peninsula arc. *Communications Earth & Environment* 5: 157, doi: 10.1038/s43247-024-01301-1

Birkenmajer K. 1982. Report on geological investigations of King George Island, South Shetland Islands (West Antarctica). *Studia Geologica Polonica* 74: 1–104.

Birkenmajer K. 1983. Strike-slip faults in the Tertiary tectonics of King George Island, South Shetland Islands (West Antarctica). *Bulletin of the Polish Academy of Sciences, Earth Sciences* 31: 21–32.

Birkenmajer K. 2002. Admiralty Bay, King George Island, South Shetland Islands, West Antarctica. Geological map 1:50 000.

Birkenmajer K. 2003. Admiralty Bay, King George Island (South Shetland Islands, West Antarctica): A geological monograph. *In:* Birkenmajer K. (ed.) *Geological results of the Polish Antarctic expeditions. Part XIV. Studia Geologica Polonica* 120: 1–-75.

Birkenmajer K., Francalanci L. and Peccerillo A. 1985. Petrology and geochemistry of volcanic rocks from Admiralty Bay, King George Island, South Shetland Islands (West Antarctica). *Bulletin of the Polish Academy of Sciences, Earth Sciences* 33: 1–15.

Blakely R.J. 1996. *Potential Theory in Gravity and Magnetic Applications*. Cambridge University Press, Cambridge.

Burton-Johnson A., Bastias J. and Kraus S. 2023. Breaking the ring of fire: How ridge collision, slab age, and convergence rate narrowed and terminated the Antarctic continental arc. *Tectonics* 42: e2022TC007634, doi: 10.1029/2022TC007634.

Catalán M., Galindo-Zaldívar J., Martín Dávila J., Martos Y.M., Maldonado A., Gambôa L. and Schreider A.A. 2013. Initial stages of oceanic spreading in the Bransfield Rift from magnetic and gravity data analysis. *Tectonophysics* 585: 102–112, doi: 10.1016/j.tecto.2012.11.018.

Espinoza Celi J.A., Cahuana-Yánez N.G., Martillo-Bustamante C.E. and González-Bonilla M. 2023. Bransfield Strait and South Shetland Islands sedimentary basement and upper crustal structure: An analysis of gravity and magnetic data at the northwestern area of the Antarctic Peninsula. *Tectonophysics* 852: 229771, doi: 10.1016/j.tecto.2023.229771.

Golynsky A.V., Ferraccioli F., Hong J.K. *et al.* 2018. New magnetic anomaly map of the Antarctic. *Geophysical Research Letters* 45: 6437–6449, doi: 10.1029/2018GL078153.

Kraus S., Koppers A.A.P., Geist D., Darvill C.M. and Duncan R.A. 2010. Geochronology of the South Shetland Islands volcanic arc: Implications for arc evolution and migration. *Geochemistry, Geophysics, Geosystems* 11: Q0AA09, doi: 10.1029/2009GC002803.

Majdański M., Środa P., Malinowski M., Czuba W., Grad M., Guterch A. and Hegedus E. 2008. 3D seismic model of the uppermost cust of Admiralty Bay area, King George Island, West Antarctica. *Polish Polar Research* 29: 303–318.

Nabighian M.N., Grauch V.J.S., Hansen R.O., LaFehr T.R., Li Y., Peirce J.W., Phillips J.D. and Ruder M.E. 2005. The historical development of the magnetic method in exploration. *Geophysics* 70: 33ND–61ND.

Nawrocki J. and Werner T. 2025. Anisotropy of magnetic susceptibility of Cretaceous to Eocene volcanic rocks from southern part of King George Island, West Antarctica. *Polish Polar Research* 46: 1–13, doi: 10.24425/ppr.2025.154564

Nawrocki J., Pańczyk M. and Williams I.S. 2010. Isotopic ages and palaeomagnetism of selected magmatic rocks from King George Island (Antarctic Peninsula). *Journal of the Geological Society, London* 167: 1063–1079.

Nawrocki J., Pańczyk M. and Williams I.S. 2011. Isotopic ages of selected magmatic rocks from King George Island (West Antarctica) controlled by magnetostratigraphy. *Geological Quarterly* 55: 301–322.

Nawrocki J., Pańczyk M., Wójcik K., Kozłowska-Roman A. 2021. Age of volcanism on Keller Peninsula and assessment of age-constrained volcanic activity on King George Island, South Shetland Islands. *Polish Polar Research* 42: 77–95, doi: 10.24425/ppr.2021.136600

Pańczyk M. and Nawrocki J. 2011. Geochronology of selected andesitic lavas from the King George Bay area (SE King George Island). *Geological Quarterly* 55: 301–322.

Pańczyk M., Nawrocki J. and Williams I.S. 2009. Late Oligocene magmatism in the Admiralty Bay area, King George Island. *Geological Quarterly* 53: 123–134.

Pankhurst R.J. and Smellie J.L. 1983. K–Ar geochronology of the South Shetland Islands, Lesser Antarctica: Apparent lateral migration of Jurassic–Cenozoic island arc volcanism. *Earth and Planetary Science Letters* 66: 214–222, doi: 10.1016/0012-821X(83)90107-5.

Smellie J.L. 2021. *Volcanism of the Antarctic Peninsula and Scotia Arc*. Springer, Cham, doi: 10.1007/978-3-030-65444-4.

Smellie J.L., Pankhurst R.J., Thomson M.R.A. and Davies R.E.S. 1984. The geology of the South Shetland Islands: VI. Stratigraphy, geochemistry and evolution. *British Antarctic Survey Scientific Reports* 87: 1–85.

Smellie J.L., Rocha-Campos A.C. and Kelley S.P. 2021. Revised stratigraphy of volcanic formations on King George Island. *Journal of Volcanology and Geothermal Research* 412: 107201, doi: 10.1016/j.jvolgeores.2021.107201.

Spector A. and Grant F.S. 1970. Statistical models for interpreting magnetic data. *Geophysics* 35: 293–302.

Tokarski A.K. 1987. Structural evolution of King George Island (South Shetland Islands, Antarctica). *Studia Geologica Polonica* 93: 7–45.

Tozer B., Sandwell D.T., Smith W.H.F., Olson C., Beale J.R. and Wessel P. 2019. Global bathymetry and topography at 15 arc sec: SRTM15+. Distributed by OpenTopography https://doi.org/10.5069/G92R3PT9 (accessed 26 January 2026).

Willan R.C.R. and Kelley S.P. 1999. Tectonic evolution of the South Shetland Islands: New constraints from geochronology. *Journal of the Geological Society* 156: 737–748, doi: 10.1144/gsjgs.156.4.0737.

Xing H., Pei J., Gao L., Wen J., Bastías J. and Zhang X. 2025. A Precambrian basement beneath the King George Island (Antarctic Peninsula) revealed by zircon xenocrystals from Eocene. *Lithos* 494–495: 107899, doi: 10.1016/j.lithos.2024.107899.

Yegorova T., Bakhmutov V., Janik T. and Grad M. 2011. Joint geophysical and petrological models for the lithosphere structure of the Antarctic Peninsula continental margin. *Geophysical Journal International* 184: 90–110, doi: 10.1111/j.1365-246X.2010.04867.x.